PERGAMON

International Journal of Solids and Structures 37 (2000) 7731–7742

INTERNATIONAL JOURNAL OF SOLIDS and STRUCTURES

www.elsevier.com/locate/ijsolstr

A semi-infinite interface crack interacting with subinterface matrix cracks in dissimilar anisotropic materials. II. Numerical results and discussion

Yi-Heng Chen *, Wen-Ye Tian

School of Civil Engineering and Mechanics, Xi'an Jiaotong University, Xi'an, Shaanxi 710049, People's Republic of China

Received 30 September 1998; in revised form 27 February 2000

Abstract

Based on the investigation performed in Part I of this series, numerical results for the interaction between a semi-infinite interface crack and multiple subinterface matrix microcracks in three kinds of material combinations are given in Part II. The major interaction behaviors are discussed in detail. Special attention is focused on the influences of the different material combinations, the T-stress, the orientation angles, and the location angles of the microcracks on the local stress intensity factor at the interface crack tip. In addition, the variable tendencies of the interaction effect induced from change of the distance between the interface crack tip and the centers of the microcracks are studied. It is concluded that the different material combinations introduced in this paper have little influence on the variable tendencies of the effect, but have significant influence on the effect in magnitude. Detailed comparisons of the results with those in a homogeneous orthotropic material show that the dissimilar materials shift the maximum amplification angle, the maximum shielding angle, the neutral shielding angle, and the neutral T-stress angle, respectively.

Keywords: Interaction behavior; T-Stress; Stress intensity factor; Material combination

1. Introduction

In Part I of this series (Tian and Chen, 2000), the interaction problem between a semi-infinite interface macrocrack and multiple subinterface matrix microcracks in dissimilar anisotropic materials has been deduced to a system of singular integral equations, which are solved numerically. Of great interest is the fact that a consistency check based on the conservation law of the J_k vector is developed, which could be used as a necessary condition for confirming the correctness and reliability of numerical results derived in this series.

In order to give a fundamental understanding of the interaction behaviors, numerical results for different dissimilar material combinations will be studied and discussed in detail in this part. Here, three

* Corresponding author. Tel.: +86-29-266-0404; fax: +86-29-323-7910.
E-mail address: yhchen2@xjtu.edu.cn (Y.-H. Chen).

0020-7683/00/$ - see front matter
PII: S0020-7683(00)00118-9

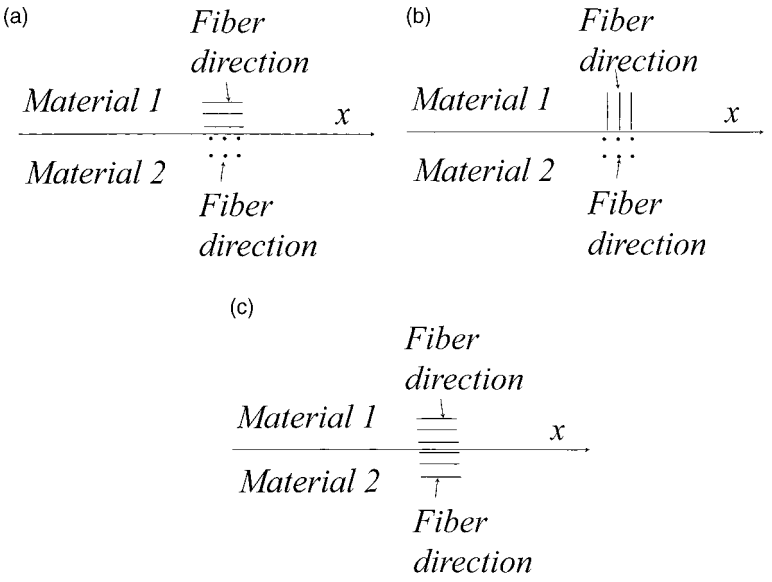

Fig. 1. Forms of the material configuration.

kinds of material combinations are considered. The first is associated with a special dissimilar composite (labeled as Case I in Fig. 1(a)) whose upper material is a unidirectional fiber reinforced composite with the fiber direction parallel to the interface and whose lower material is the same composite but with the fiber direction perpendicular to the considered plane (i.e., a 90°/0° layered composite). Therefore, matrix cracks near the tip of an interface crack are more likely to be formed in the lower material. The second is associated with another kind of material combination (labeled as Case II in Fig. 1(b)) whose upper material is also the unidirectional fiber reinforced composite mentioned above, but its fiber direction is perpendicular to the interface and whose lower material is the same composite and its fiber direction is perpendicular to the considered plane (another kind of layered composite). The third case is specially introduced for comparison, which is associated with a homogeneous orthotropic material (labeled as Case III in Fig. 1(c)), i.e., the whole plane is occupied by the composite with the fiber direction parallel to the semi-infinite crack. Special attention is focused on the influences on the macrocrack–microcrack interaction effect (described by the local stress intensity factor (SIF)) induced from the different material combinations, the orientation angles and the location angles of subinterface microcracks, the normalized distance between the interface macrocrack tip and the centers of subinterface microcracks, and the remote T-stress. In Section 2 of this part, the interaction behaviors between a semi-infinite interface macrocrack and one single subinterface microcrack are studied in detail. Numerical results reveal that the three kinds of material combinations mentioned above have little influence on the variable tendencies of the interaction effect, but have significant influence on the amplitude of the effect. The change of material combinations from a homogeneous material to a dissimilar material shifts the maximum amplification angle, the maximum shielding angle, and the neutral shielding angle. In Section 3, two microcracks in the near-tip stress field of a macrointerface crack are considered. Not only the interaction between the macrocrack and the microcracks, but also the interaction between the two microcracks are taken into account. It is seen that the same conclusion could be given as those derived in Section 2. It is concluded that the influence of different material combinations yields to shift the location angle at which the maximum or minimum interacting effect occurs and to change the maximum or minimum values of the

effect as well. The variable tendencies of the energy release rate at the interface crack tip are also plotted in figures, which show similar natures to those of the local SIF. In Section 4, the effect of the T-stress is considered. It is shown that these conclusions obtained in homogeneous isotropic materials (Zhao and Chen, 1998a,b) are still valid in present interaction problem.

2. One single microcrack in the near-tip stress field

In this section, one single subinterface microcrack in the near-tip process zone of an interface crack is considered as shown in Fig. 4 of Part I of this series. In order to give a fundamental understanding of the interaction behaviors between the microcrack and the interface crack, three kinds of material combinations are considered as shown in Fig. 1(a)–(c), respectively. The material constants of the single phase have been used in Part I of this series. As the value of the mismatch index is always extremely small for Cases I and II ($\varepsilon = 0.019$), the remote stress field is specified by the purely Mode I SIF K_1^∞ with $K_2^\infty = 2\varepsilon K_1^\infty$ at the interface crack tip and the local SIF $K_1^t = K_1^\infty + \Delta K_1$ at the interface crack tip is normalized by K_1^∞ only.

Numerical results of the normalized local SIF $(K_1^\infty + \Delta K_1)/K_1^\infty$ at the interface crack tip against the location angle α of a parallel microcrack ($\beta = 0^\circ$) are shown in Fig. 2(a)–(c), where the normalized distance r/a is, respectively, taken to be 2.0, 2.2, and 2.5. It is found that the variable tendencies of the dotted curves, the imaginary curves, and the real curves corresponding to the three kinds of material combinations labeled as Cases I–III, are similar. When the location angle α increases from 10°, in all three cases, the value of the local SIF increases until the maximum amplification effect reaches. The corresponding value of the angle α is called the maximum amplification angle. The value of the local SIF decreases as the angle α increases from the maximum amplification angle until the neutral shielding angle reaches (Gong and Horii, 1989). Then, the value of the local SIF decreases further as the angle α increases until the maximum shielding effect reaches. The corresponding value of the angle α is called the maximum shielding angle. Furthermore, the value of the local SIF increases as the angle α increases. However, the changes of the interaction effect in magnitude among the three kinds of material combinations described by $(K_1^\infty + \Delta K_1)/K_1^\infty$ are remarkable. Particularly, the dissimilar composite materials shift the maximum amplification angle, the maximum shielding angle, and the neutral shielding angle, respectively. In other words, the values of the maximum amplification angles and the maximum shielding angles in Cases I and II corresponding to dissimilar anisotropic materials mentioned above are always larger than those in Case III corresponding to a homogeneous orthotropic material. However, the neutral angles in Cases I and II are always a little less than those in Case III. For example, in Fig. 2(a), the values of the maximum amplification angle (at which the maximum amplification effect occurs) in Cases I and II are about 29°, while the value in Case III is about 24°; the values of the maximum shielding angle (at which the maximum shielding effect occurs, Ortiz (1989)) in Cases I and II are 109°, while the value in Case III is 104°; the values of the neutral shielding angle (at which a transformation from the amplification to the shielding effect occurs, Gong and Horii (1989)) in Cases I and II are 65°, while the value in Case III is 67°. It is concluded that the material mismatch nature induced from the two dissimilar composite materials (Case I or Case II) always decreases the neutral shielding angle and in turn to increase the shielding region near the macrocrack tip in the lower half-plane. What is more, the values of $(K_1^\infty + \Delta K_1)/K_1^\infty$ in Case III (homogeneous orthotropic material) at the maximum amplification angle are much smaller than those in Cases I and II. Quite contrary, the values of $(K_1^\infty + \Delta K_1)/K_1^\infty$ in Case III at the maximum shielding angle are much greater than those in Cases I and II. This means that the material mismatch induced from Cases I and II increases the interaction effect due to the existence of the interface, whatever the microcrack is formed in the amplification region or shielding region.

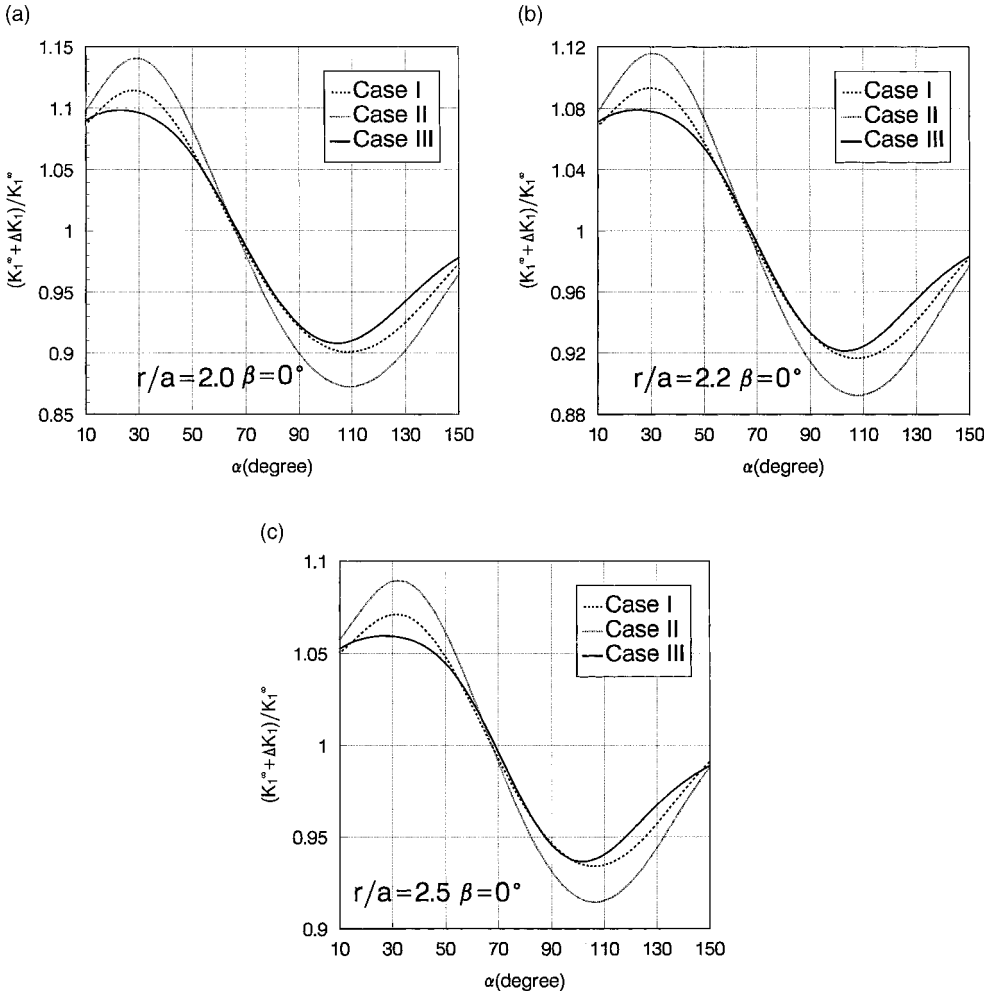

Fig. 2. Normalized SIF $(K_1^{\infty} + \Delta K_1)/K_1^{\infty}$ vs. the angle α: (a) $r/a = 2.0$, (b) $r/a = 2.2$ and (c) $r/a = 2.5$.

Numerical results of $(K_1^{\infty} + \Delta K_1)/K_1^{\infty}$ against the orientation angle β of the microcrack are shown in Fig. 3(a)–(c), where the location angle α is taken to be 60°, 90°, and 120°, respectively. It is found that the variable tendencies of the dotted curves (Case I), the imaginary curves (Case II), and the real curves (Case III), are also similar. However, in most range of β, the divergencies in magnitude of the effects in Cases I and II from those in Case III are remarkable. It is seen from Fig. 3(a) and (b) that, the homogeneous orthotropic material corresponding to Case III does always lead to smaller values of the effect than those for Cases I and II when the maximum amplification effect occurs. For example, in Fig. 3(a), the values of the interaction effect at the maximum amplification angles are 1.185 in Case I, 1.235 in Case II, and 1.18 in Case III. In Fig. 3(b), the values of the interaction effect at the maximum amplification angles are 1.093 in Case I, 1.13 in Case II, and 1.086 in Case III. However, such a behavior is not a general phenomenon for every case. For example, the above phenomenon could not be seen in Fig. 3(c), where the value of the maximum amplification effect corresponding to Case III is obviously greater than that corresponding to Case I, although it is smaller than that corresponding to Case II. In addition, it could be seen that the

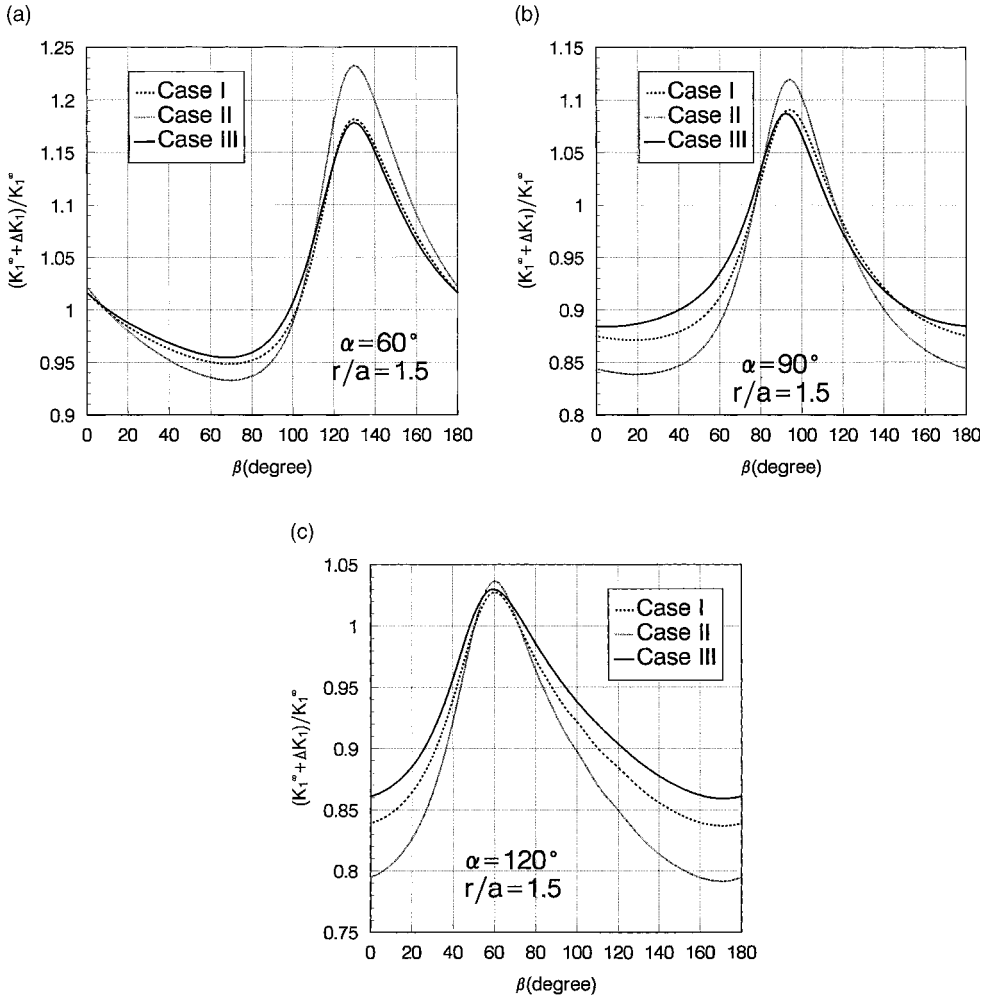

Fig. 3. Normalized SIF $(K_1^{\infty} + \Delta K_1)/K_1^{\infty}$ vs. the angle β: (a) $\alpha = 60°$, (b) $\alpha = 90°$ and (c) $\alpha = 120°$.

maximum amplification angles in Fig. 3(b) are 95° for Cases I and II, and 92° for Case III. Thus, as concluded above, the material mismatch nature on the interface induced from dissimilar materials shown in Fig. 1(a) and (b) shifts the maximum amplification angle and in turn shifts the amplification region below the interface.

Numerical results of the energy release rate are also plotted in this section. Here, the energy release rate at the interface crack tip is formulated as (Suo, 1990)

$$G_t = J_t = \overline{\mathbf{w}}^{\mathrm{T}}(\mathbf{H} + \overline{\mathbf{H}})\mathbf{w}\left|K_1^{\infty} + \Delta K_1 + \mathrm{i}(K_2^{\infty} + \Delta K_2)\right|^2/(4\cosh^2\pi\varepsilon) \tag{1}$$

which is normalized by (Suo, 1990)

$$G_{\infty} = J_{\infty} = \overline{\mathbf{w}}^{\mathrm{T}}(\mathbf{H} + \overline{\mathbf{H}})\mathbf{w}\left|K_1^{\infty} + \mathrm{i}K_2^{\infty}\right|^2/(4\cosh^2\pi\varepsilon). \tag{2}$$

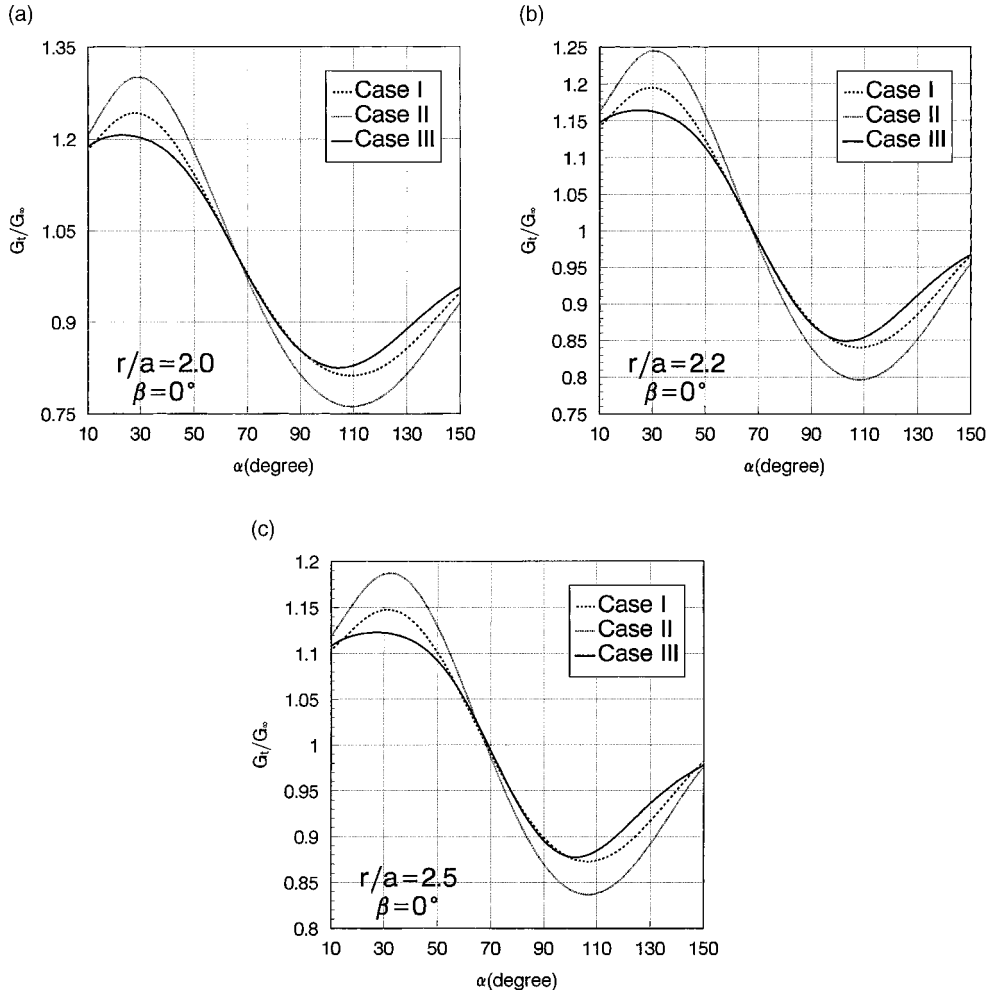

Fig. 4. Normalized energy release rate G_t/G_∞ vs. the angle α: (a) $r/a = 2.0$, (b) $r/a = 2.2$ and (c) $r/a = 2.5$.

As could be seen in Fig. 4(a)–(c) for the parallel microcrack, when taking the energy release rate as the measure of the interaction effect, the variable tendencies of the three kinds of curves are similar to those shown in Fig. 2(a)–(c).

For the inclined microcrack with β to be variable from 0° to 180°, the curves of G_t/G_∞ in Fig. 5(a)–(c) shows the similar variable tendencies to those in Fig. 3(a)–(c). Indeed, the energy release rate at the interface crack tip leads to the same behaviors of the interaction effect as those derived by the local SIF under nearly purely Mode I remote loading conditions, i.e., $K_1^\infty \gg K_2^\infty$.

This is due to the two well-known facts that the values of the SIF $K_1^\infty + \Delta K_1$ are much larger than those of ΔK_2 at the interface crack tip under the present case and the diagonal elements in matrix **H** of Eq. (1) take the overwhelming positions in comparison with the non-diagonal elements. It should be emphasized that, this conclusion may no longer be valid when the really combined Modes I and II remote loading conditions are specified (K_1^∞ and K_2^∞ take the same order in magnitude) or when the material mismatch yields the same order in magnitude for both the diagonal elements and the non-diagonal elements in matrix **H**.

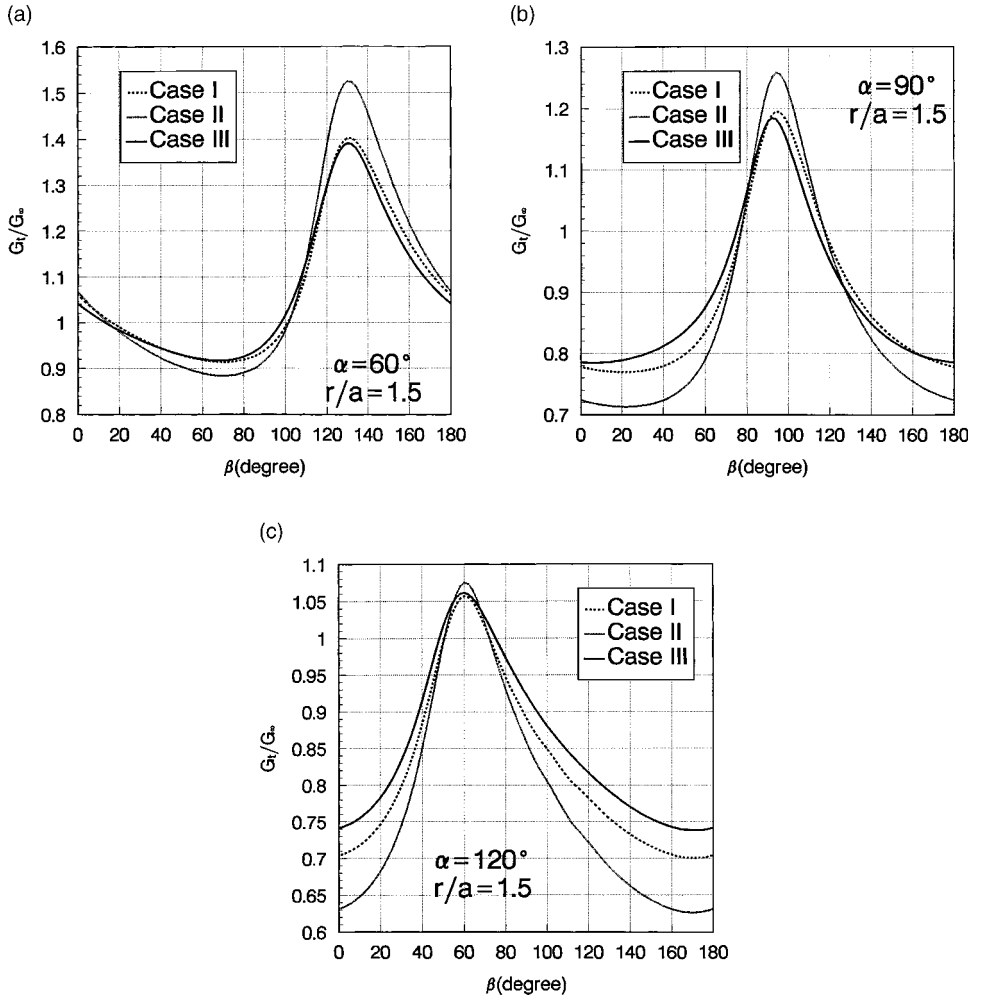

Fig. 5. Normalized energy release rate G_t/G_∞ vs. the angle β: (a) $\alpha = 60°$, (b) $\alpha = 90°$ and (c) $\alpha = 120°$.

3. Two microcracks in the near-tip stress field

Consider a semi-infinite interface crack interacting with two microcracks of length $2a$ in the near-tip stress field. The remote stress field is still specified by K_1^∞ with $K_2^\infty = 2\varepsilon K_1^\infty$ as shown in Fig. 6. Here, α_1 and α_2, β_1 and β_2, r_1 and r_2, are the location angles, the orientation angles, the distances of the microcracks 1 and 2, respectively. Fig. 7 shows the variable tendencies of the local SIF against the orientation angle β_1 of the microcrack 1, taking $\alpha_1 = 45°$, $\alpha_2 = 135°$, and $\beta_2 = 0$, $r_1/a = r_2/a = 2$, respectively. It should be emphasized that, in the present case, not only the interaction between the macrointerface crack and the microcracks, but also the interaction between the two microcracks is taken into account.

It is seen that the conclusion derived in one single microcrack case is still valid in two microcracks case, i.e., the variable tendencies of the curves of the interaction effect $((K_1^\infty + \Delta K_1)/K_1^\infty)$ corresponding to the three kinds of material combinations labeled as Cases I–III are similar. However, in most range of β_1, the changes of the interaction effect in magnitude described by $(K_1^\infty + \Delta K_1)/K_1^\infty$ corresponding to different

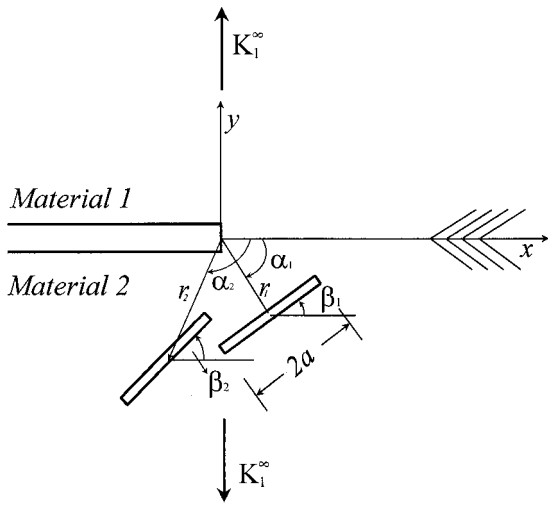

Fig. 6. A semi-interface crack and two microcracks.

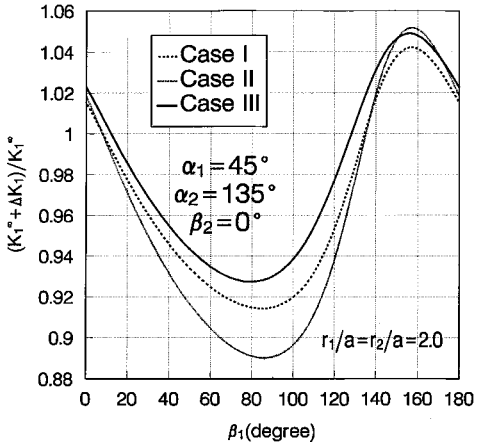

Fig. 7. Normalized SIF $(K_1^\infty + \Delta K_1)/K_1^\infty$ vs. the angle β_1.

material combinations are remarkable. It is also seen that the dissimilar composite materials (Cases I and II) shift the maximum amplification angle, the maximum shielding angle and the neutral shielding angle from those for the homogeneous composite material (Case III). For example, the value of the maximum shielding angle is 86° for Cases I and II, 80° for Case III.

4. Effect of the T-stress

As known, besides the local SIF, the T-stress effect has received much attention in the analysis of fracture. In the notation of Rice (1974), the stress distribution in the vicinity of a macrocrack tip could be expressed in the cylindrical coordinates (r, θ) as follows:

$$\begin{bmatrix} \sigma_{11} & \sigma_{12} \\ \sigma_{21} & \sigma_{22} \end{bmatrix} = \frac{K}{\sqrt{2\pi r}} \begin{bmatrix} f_{11}(\theta) & f_{12}(\theta) \\ f_{12}(\theta) & f_{22}(\theta) \end{bmatrix} + \begin{bmatrix} T & 0 \\ 0 & 0 \end{bmatrix} + 0(\sqrt{r}), \tag{3}$$

where the second term of Eq. (3) denoted by the T-stress is regarded as a stress acting parallel to the crack plane.

In the above section, only the first term corresponding to the SIF in Eq. (3) is discussed with no regards to the second term corresponding to the T-stress. Although Zhao and Chen (1998a,b) have studied the T-stress effect for the macrocrack–microcrack interaction problem in isotropic materials and in metal/ceramic bimaterials, the effect in the present problem in dissimilar anisotropic materials remains to be investigated.

In this section, special attention is focused on the coupled nature between the remote T-stress and the material mismatch nature in the three material combinations mentioned above. As treated by Leevers and Radon (1983) and Betegon and Hancock (1991), the magnitude of the remote T-stress denoted by T^{∞} is defined through a biaxiality parameter B:

$$B = \frac{T^{\infty}\sqrt{\pi a}}{K_1^{\infty}}, \tag{4}$$

where a is half of the mean length of the N microcracks in the process zone of the lower half-plane for a semi-infinite interface crack:

$$a = \sum_{i=1}^{N} \frac{a_i}{N}, \tag{5}$$

and a_i is the half-length of the ith microcrack.

Consider the problem shown in Fig. 8, where a subinterface microcrack of length $2a$ is just centered below the macrocrack tip. The remote stress field is specified by K_1^{∞}, $T^{\infty u}$ and T^{∞}, keeping in mind that the K_2^{∞} is quite small and related with K_1^{∞} and the $T^{\infty u}$-stress and T^{∞}-stress on the upper half-plane and the lower half-plane are different in Cases I and II, and are the same in Case III.

Computed values of the normalized SIF $(K_1^{\infty} + \Delta K_1)/K_1^{\infty}$ vs. the oriented angle β are shown in Fig. 9(a) and (b). It is assumed that $B = -0.5$ and –1.0 in Fig. 9(a) and $B = 0.5$ and 1.0 in Fig. 9(b). It is found that,

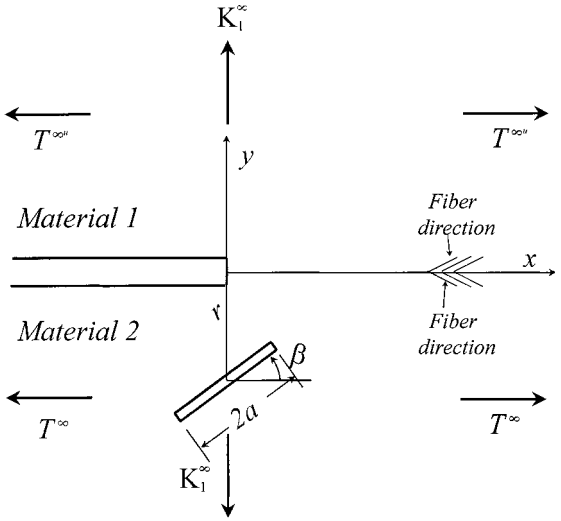

Fig. 8. A macrocrack interacting with a subinterface microcrack centered just below the macrocrack tip.

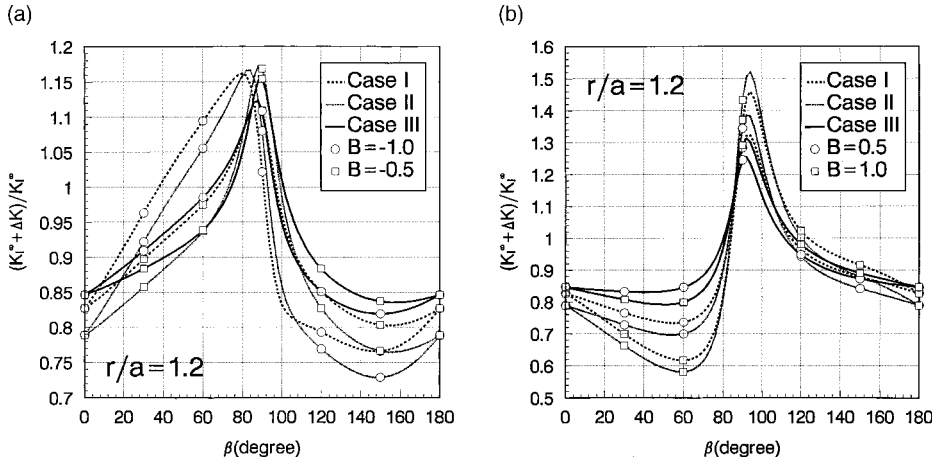

Fig. 9. Normalized SIF $(K_{\mathrm{I}}^{\infty}+\Delta K_{\mathrm{I}})/K_{\mathrm{I}}^{\infty}$ vs. the angle β after considering the T-stress: (a) $B=-0.5$ and $B=-1.0$; (b) $B=0.5$ and $B=1.0$.

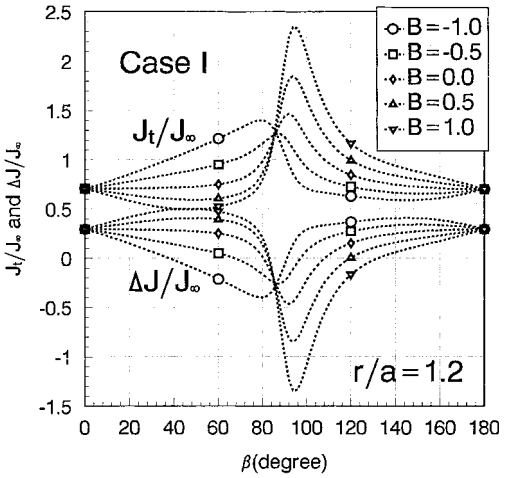

Fig. 10. The J-integral vs. the angle β for Case I after considering the T-stress.

for the parallel microcrack corresponding to $\beta=0^{\circ}$ and $\beta=180^{\circ}$, the remote T-stress has little influence on the SIF although the Modes I and II fractures are coupled in the near-tip stress field due to the mismatch nature. It is found also that the T-stress has significant influence on the local SIF for an oriented microcrack. Moreover, the influence is sensitive to the material combinations although the variable tendencies of the influence induced by T^{∞} in the three cases are similar. The transformation angle β_{T} from which the T-stress yields opposite influences on SIF is about 87° no matter how the material combinations are considered and whatever T^{∞} is negative corresponding to $B<0$ or positive corresponding to $B>0$. However, the influence of the material combinations on the SIF in magnitude for a certain value of T^{∞} is remarkable. For example, it is seen in Fig. 9(a) that the maximum value of SIF is about 1.16 for Case I at $\beta=80^{\circ}$, 1.17 for Case II at $\beta=84^{\circ}$, and 1.125 for Case III at $\beta=88^{\circ}$, when taking $B=-1.0$. Also, the minimum value of SIF is about 0.765 for Case I at $\beta=150^{\circ}$, 0.73 for Case II at $\beta=150^{\circ}$, and 0.82 for Case III at $\beta=150^{\circ}$.

It is concluded that the divergencies of the influence of T^{∞} on SIF for the two dissimilar cases from those for the orthotropic case are remarkable, but the divergencies of Case I from Case II are smaller. Similar conclusions could also be given in Fig. 9(b) although T^{∞} is positive.

The influence of T^{∞} on the redistribution of the J-integral is plotted in Fig. 10 for Case I only. It is found that, although T^{∞} influences the redistribution of the J-integral significantly, the consistent relation (33) in Part I is still valid whatever the values of T^{∞} are positive or negative. This conclusion is identical with those obtained in homogeneous isotropic material (Zhao and Chen, 1998). It should be pointed out that the numerical results for Cases II and III also meet the consistent relation of the J-integral. Here, the computed values in these two cases would not be shown any more for shortening the length of this paper.

5. Conclusion remarks

Although only the three typical examples are considered in this part, the numerical results and discussion do provide a fundamental understanding of the influence of the near-tip microstructure on the dominant parameters at an interface crack tip in dissimilar composite materials, such as the local SIF and the energy release rate. The major conclusions could be summarized as follows:

(1) The variable tendencies of the interaction effect in the present dissimilar composite materials are similar to those in orthotropic materials with the stiffer axis parallel to the macrocrack. This means that the material mismatch nature at the interface crack tip has little influence on the variable tendencies of the effect when the remote stress field is specified by the nearly Mode I K_{I}^{∞}. However, the divergencies of the effect in magnitude from those in orthotropic materials are remarkable.

(2) The material mismatch nature on the interface shifts the maximum amplification angle, the maximum shielding angle, and the neutral shielding angle, at which the maximum amplification effect occurs, the maximum shielding effect occurs, and a transformation from the amplification effect to the shielding effect occurs, respectively.

(3) The energy release rate at the interface crack tip plays the same role as that of the local SIF in the present interaction problem when the remote stress field is the nearly purely Mode I and the material mismatch yields the overwhelming diagonal elements in the matrix $\mathbf{H}$.

(4) The T-stress does bring great influences on the interaction behaviors between interface macrocrack and subinterface microcracks. However, after considering the T-stress, the consistent relation of the J-integral, i.e., Eq. (33) in Part I, is still satisfied.

Acknowledgements

This work was supported by the Chinese National Natural Science Foundation.

References

Betegon, C., Hancock, J.W., 1991. Two-parameter characterization of elastic plastic crack-tip fields. ASME J. Appl. Mech. 58, 104–110.

Gong, S.X., Horii, H., 1989. General solution to the problem of microcracks near the tip of a main crack. J. Mech. Phys. Solids 37, 27–46.

Leevers, P.S., Radon, J.C., 1983. Inherent stress biaxiality in various fracture specimen geometries. Int. J. Fract. 19, 311–325.

Ortiz, M., 1989. Maximal crack tip shielding by microcracking. ASME J. Appl. Mech. 56, 279–283.

Rice, J.R., 1974. Limitations to the small scale yielding approximation for crack tip plasticity. J. Mech. Phys. Solids 22, 17–26.

Suo, Z.G., 1990. Singularities, interface and cracks in dissimilar anisotropic media. Proc. R. Soc. Lond. A427, 331–358.

Tian, W.Y., Chen, Y.H., 2000. A semi-infinite interface crack interacting with subinterface matrix cracks in dissimilar anisotropic materials. Part I. Fundamental formulations and the *J*-Integral Analysis. Int. J. Solids Struct. 37, 7717–7730.

Zhao, L.G., Chen, Y.H., ASME, J., 1998a. Effect of the T-stress in microcrack shielding problems. J. Appl. Mech. 65, 71–75.

Zhao, L.G., Chen, Y.H., 1998b. T-stress of an interface macrocrack induced by near-tip subinterface microcracks. Int. J. Fract. 1 (90), 275–285.